

# PLCReg: Correlation-Aware Polar-Linear Attention for Guiding Medical Image Registration

## Supplementary Material

### 7. Complexity Analysis

Given a 3D medical image input of size  $H \times W \times D$ , it is partitioned into  $M$  patches. Let  $d$  denote the number of channels per attention head (total channels  $C = h \cdot d$ ),  $d'$  the dimensionality after feature mapping (element-wise mapping yields  $d' = d$ ), and  $k \times k \times k$  the 3D convolution kernel size. The computational cost of a single-head attention can be decomposed as follows: 1) the linear projections to generate  $\mathbf{Q}$ ,  $\mathbf{K}$ ,  $\mathbf{V}$ , the polarity fusion coefficient matrix  $\mathbf{G}$ , and the output projection cost  $5Md^2$ ; 2) polarity-aware linear attention includes four computational paths with cost  $4Mdd'$ ; 3) depthwise separable convolution costs  $k^3Md$ ; 4) the element-wise gating product of  $\mathbf{G}$  with the correlated features costs  $Md$ . Therefore, the single-head complexity is:

$$\Omega_{3D} = 5Md^2 + 4Mdd' + k^3Md + Md \quad (12)$$

With multiple attention heads, the total complexity is  $h \cdot \Omega_{3D}$ , which remains linear in the sequence length  $M$ .

### 8. Dataset Details

Our experiments use three publicly available 3D brain MRI datasets—LPBA40, OASIS, and IXI—and a multimodal brain CT–MR dataset, SR-Reg. The preprocessed LPBA40 dataset contains 40 T1-weighted MRI scans from healthy subjects ( $160 \times 192 \times 160$ ), split into 30 training cases and 9 test cases, with the remaining 1 case used as an atlas for atlas-based registration. Each MRI scan is rigidly pre-aligned to the MNI305 template and has 54 anatomical labels for evaluation. The OASIS dataset includes 414 brain scans and 35 manually labeled anatomical structures, preprocessed with FreeSurfer and SAMSEG to obtain skull-stripped and bias-corrected 3D images of size ( $160 \times 224 \times 192$ ). The dataset is split into training/test counts of [394, 19], with 1 remaining scan used as an atlas. The IXI dataset consists of 576 T1-weighted brain MRI scans ( $160 \times 192 \times 224$ ), split into 403 training, 58 validation, and 115 test cases, following the same partition as in TransMorph. We use 30 anatomical structures as ground truth for evaluation. SR-Reg is derived from the SynthRAD 2023 Challenge dataset and includes 180 paired CT–MR volumes, each pair belonging to the same subject. We split the data into 150 training, 10 validation, and 20 test cases for inter-subject cross-modal registration.

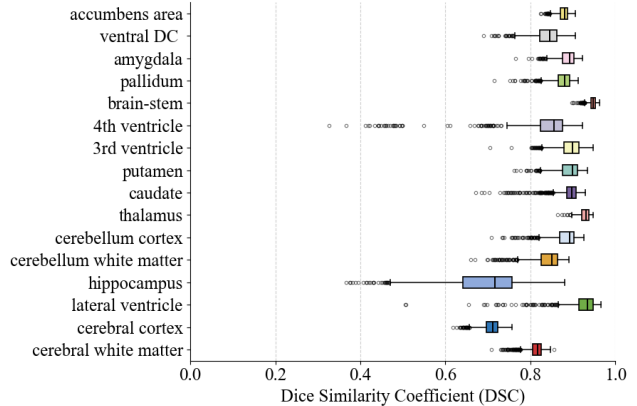


Figure 6. Boxplots of DSC scores for 16 labeled anatomical structures on the SR-Reg dataset.

### 9. P-Value Details

As shown in Tab. 6, on the LPBA40 dataset, based on 9 paired samples, PLCReg achieves consistently significant advantages over seven representative baselines according to two-sided Wilcoxon signed-rank tests ( $p \leq 0.05$ ). The typical (median) gain is 1%~4.4%, and the average relative improvement in DSC over TransMatch, TransMorph, VoxelMorph, and CycleMorph is approximately 6%~7%, indicating stable superiority both statistically and in practice. On the OASIS dataset, based on 19 paired samples, two-sided Wilcoxon signed-rank tests ( $p \leq 0.05$ ) likewise confirm the significant advantage of PLCReg. On the IXI dataset, with 115 paired samples, the results similarly demonstrate that our proposed PLCReg exhibits significant advantages. Tab. 7 also shows that our method has significant advantages.

### 10. Additional Results

Fig. 6, Fig. 7, Fig. 8, and Fig. 9 present box plots of DSC distributions across anatomical structures on the LPBA40, OASIS, IXI, and SR-Reg datasets, respectively. Our proposed PLCReg attains higher DSC on most structures and exhibits narrower interquartile ranges (IQR), indicating improved model stability.

Fig. 10, Fig. 11, Fig. 12, and Fig. 13 provide additional qualitative results on the LPBA40, OASIS, IXI, and SR-Reg datasets, respectively, as shown on the following pages.

Table 6. P-Value detailed data on DSC. The n-pairs represents the number of pairs of samples participating in the pairing, median-diff represents the median after the sample difference, which is used to measure the typical magnitude of improvement, and p-value is the two-sided p-value of the Wilcoxon signed-rank test.

Compare Method	LPBA40			OASIS			IXI		
	n-pairs	median-diff	p-value	n-pairs	median-diff	p-value	n-pairs	median-diff	p-value
VoxelMorph	9	0.0435597	0.003906	19	0.0558277	6.10351e-5	115	0.0130474	1.31286e-20
CycleMorph	9	0.0425499	0.003906	19	0.0537520	6.10351e-5	115	0.0146259	1.31286e-20
TransMorph	9	0.0400447	0.003906	19	0.0389305	6.10351e-5	115	0.0079800	1.31286e-20
TransMatch	9	0.0378704	0.003906	19	0.0429190	6.10351e-5	115	0.0106991	1.34779e-20
OFG	9	0.0357452	0.003906	19	0.0352896	6.10351e-5	115	0.0085649	1.31286e-20
CGNet	9	0.0151406	0.003906	19	0.0313991	6.10351e-5	115	0.0074458	1.53675e-20
SACBNet	9	0.0100340	0.003906	19	0.0164982	6.10351e-5	115	0.0075193	1.93753e-15

Table 7. P-Value detailed data on HD95. The n-pairs represents the number of pairs of samples participating in the pairing, median-diff represents the median after the sample difference, which is used to measure the typical magnitude of improvement, and p-value is the two-sided p-value of the Wilcoxon signed-rank test.

Compare Method	LPBA40			OASIS			IXI		
	n-pairs	median-diff	p-value	n-pairs	median-diff	p-value	n-pairs	median-diff	p-value
VoxelMorph	9	1.0105885	0.003906	19	0.2706419	6.10351e-5	115	0.0475958	3.32905e-06
CycleMorph	9	1.1233047	0.003906	19	0.2543114	6.10351e-5	115	0.0904326	4.39490e-12
TransMorph	9	0.9852025	0.003906	19	0.1092687	0.00115966	115	0.0028240	0.039952745
TransMatch	9	1.0718779	0.003906	19	0.1380846	0.00042724	115	0.0067111	0.015304258
OFG	9	0.8836315	0.003906	19	0.0991653	0.00115966	115	0.0026227	0.047623956
CGNet	9	0.6979807	0.003906	19	0.0710048	0.00671386	115	-0.006563	0.237805632
SACBNet	9	0.1315512	0.003906	19	0.1423584	0.00018310	115	0.1112194	8.49234e-18

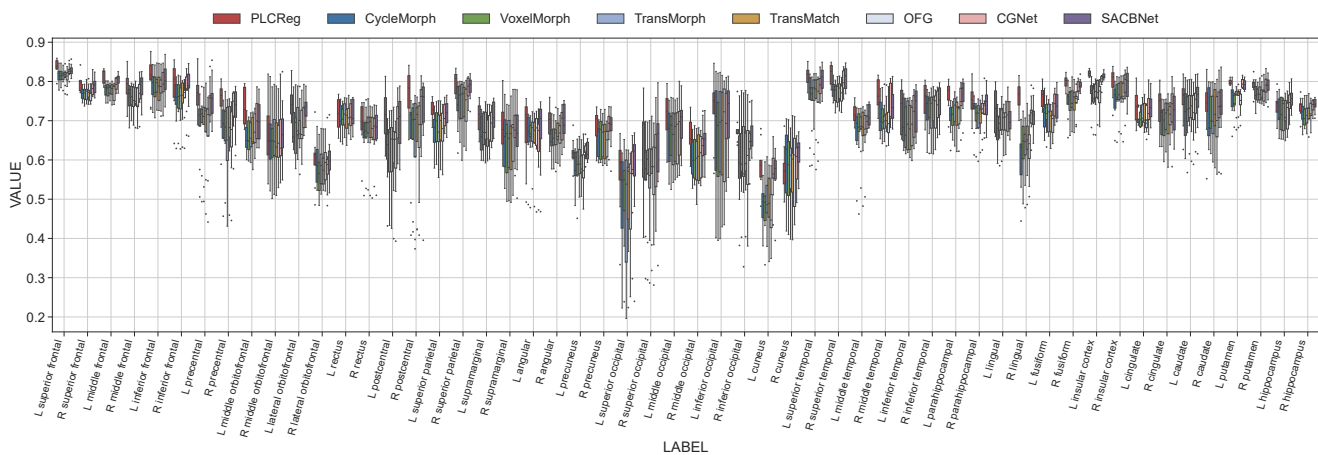


Figure 7. Boxplots show the DSC scores of our PLCReg method and the comparison method on 54 anatomical structures on the LPBA40 dataset.

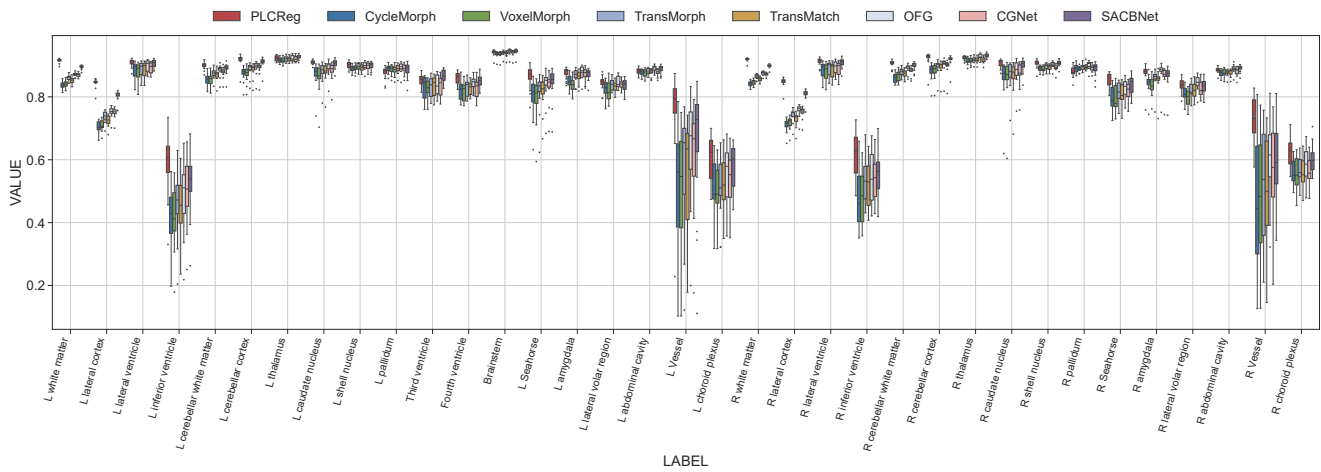


Figure 8. Boxplots show the DSC scores of our PLCReg method and comparative methods on 35 anatomical structures on the OASIS dataset.

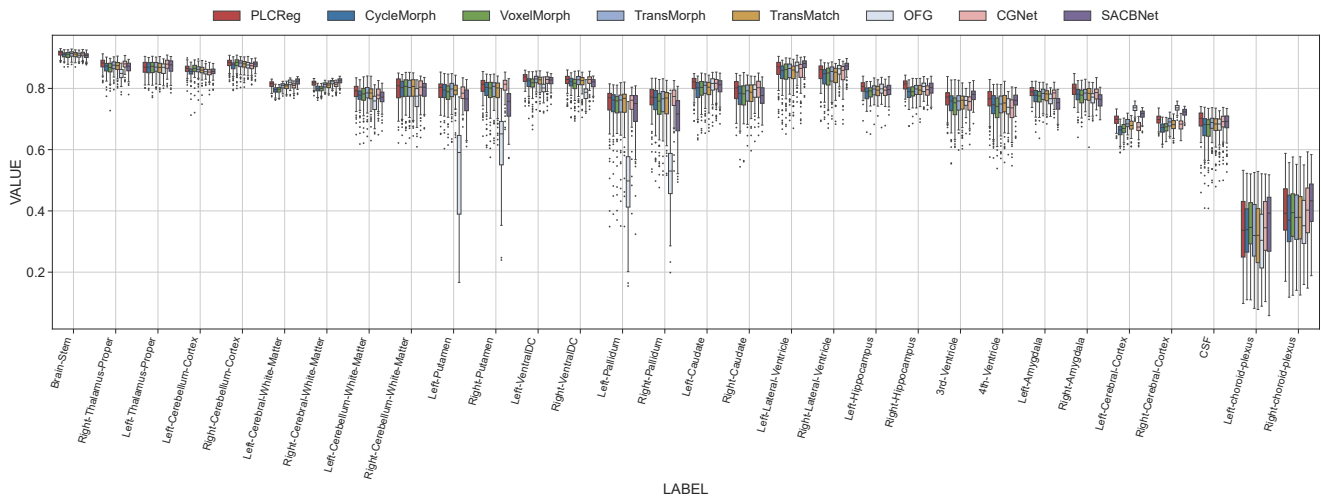


Figure 9. Box plots show the DSC scores of our PLCReg method and the comparison method on 30 anatomical structures on the IXI dataset.

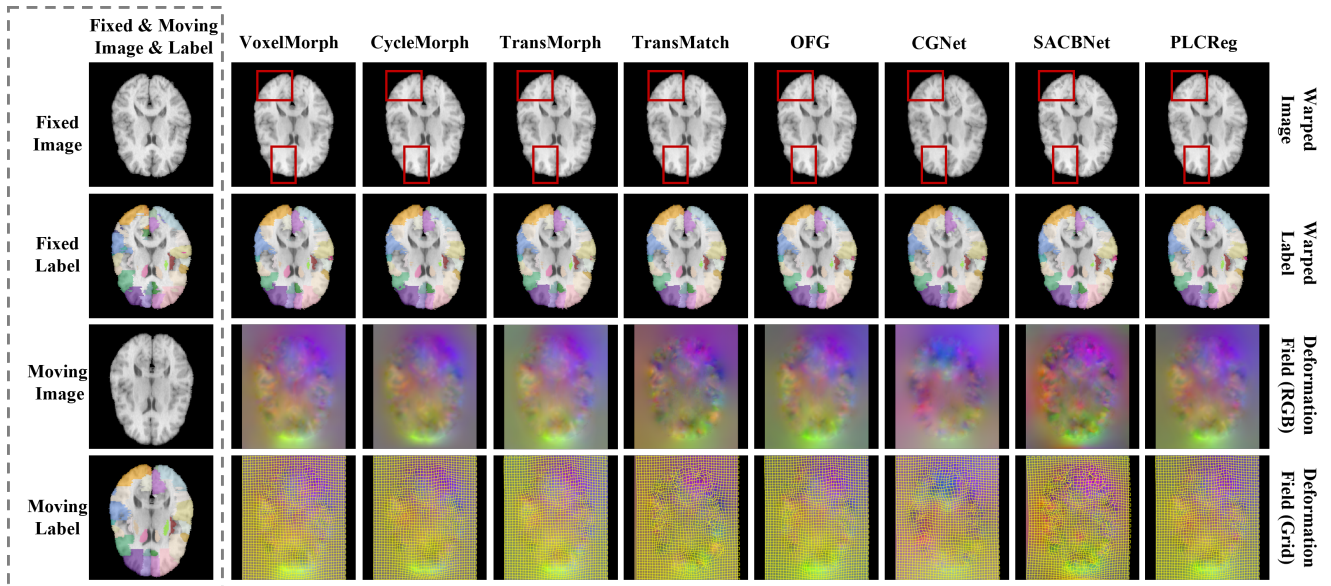


Figure 10. Visual comparison of LPBA40 dataset. The 1st and 2nd lines are the deformation map and the corresponding deformation segmentation mask map, the 3rd and 4th lines are the deformation field (RGB) and the deformation field (Grid).

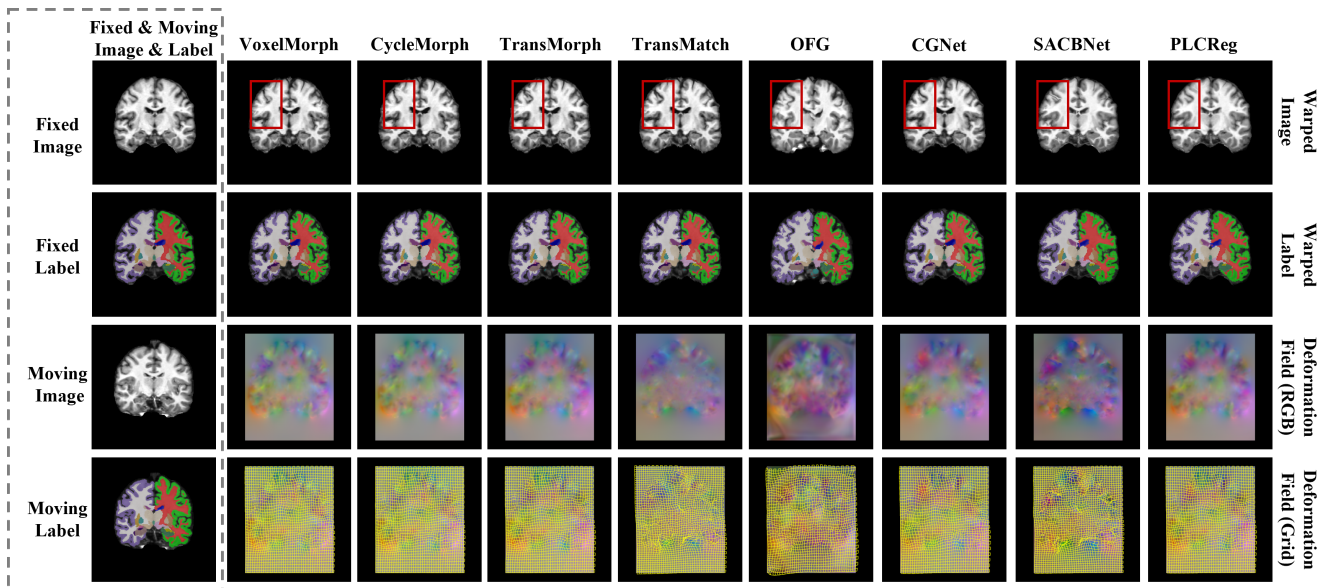


Figure 11. Visual comparison of OASIS datasets. The 1st and 2nd lines are the deformation map and the corresponding deformation segmentation mask map, the 3rd and 4th lines are the deformation field (RGB) and the deformation field (Grid).

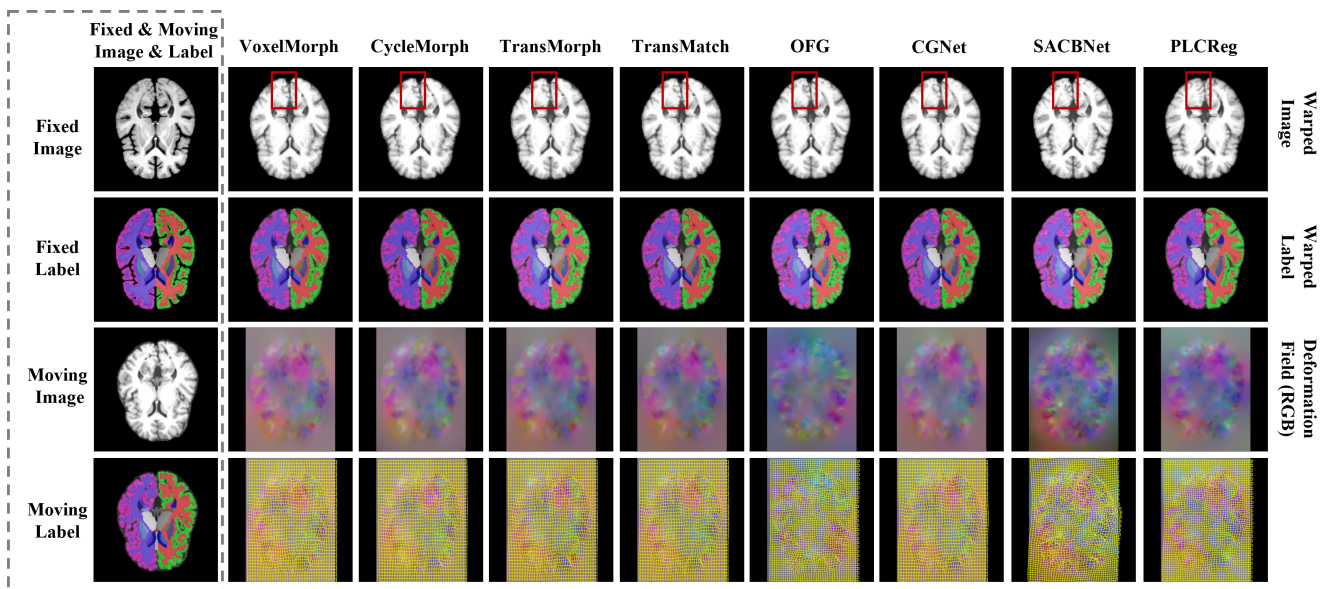


Figure 12. Visual comparison of IXI datasets. The 1st and 2nd lines are the deformation map and the corresponding deformation segmentation mask map, the 3rd and 4th lines are the deformation field (RGB) and the deformation field (Grid).

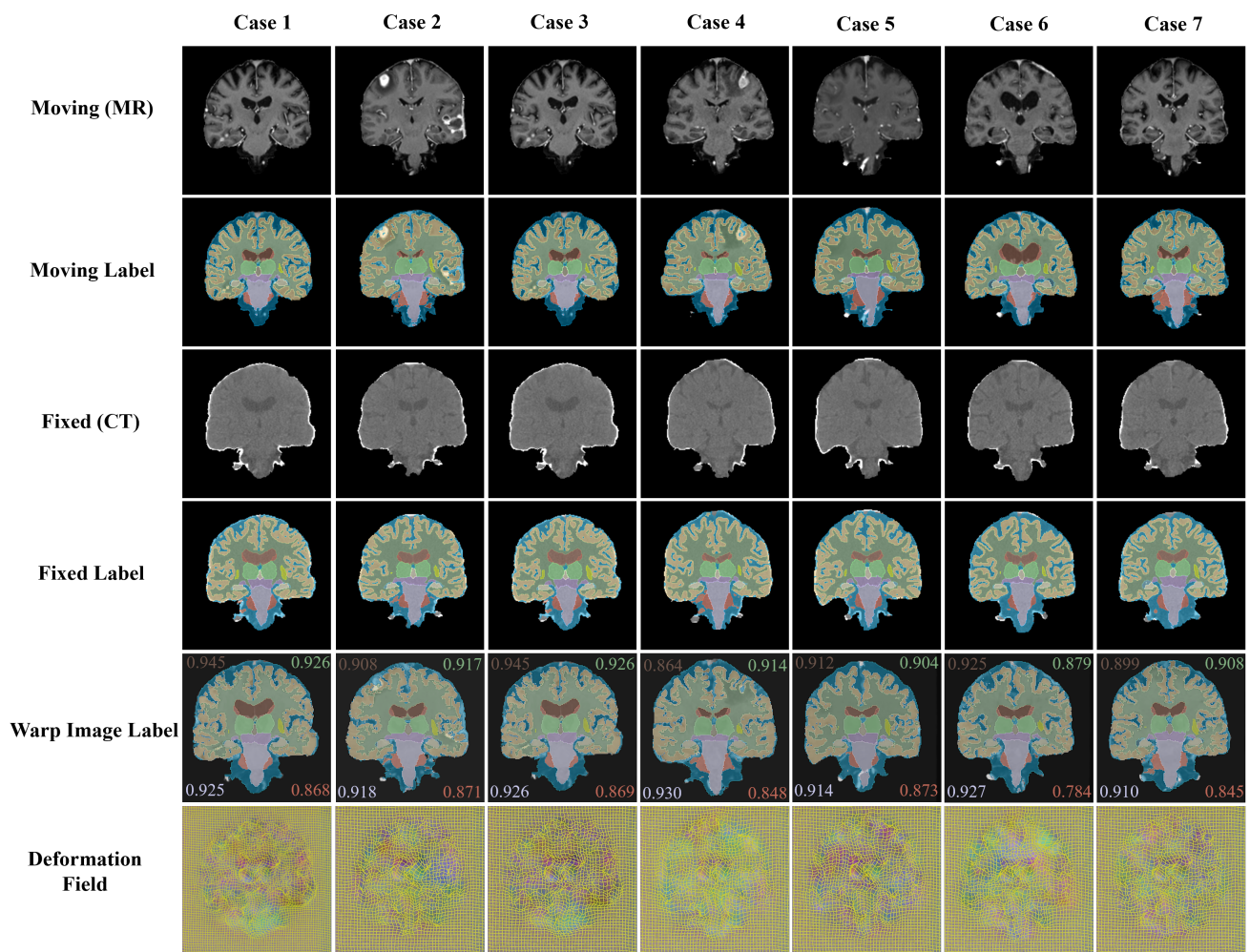


Figure 13. SR-Reg dataset visualization results. Lines 1~4 are the moving MR image, fixed CT image and their segmentation mask, lines 5 and 6 are the deformation segmentation mask and deformation field (Grid). The highlighted DSC scores are the lateral ventricles (brown), thalamus (green), brainstem (purple) and caudate nucleus (red).